Design of Hydrogel Microneedle Arrays for Interstitial Fluid Analysis and Animal Physiology Monitoring

Laurabelle Gautier , Sandra Wiart-Letort , Alexandra Massé , Caroline Xavier , Lorraine Novais-Gameiro , Antoine Hoang , Marie Escudé , Ilaria Sorrentino , Muriel Bonnet , Florence Gondret , Claire Verplanck , Isabelle Texier *

Posted Date: 29 July 2025

doi: 10.20944/preprints202507.2400.v1

Keywords: microneedles; animal health and welfare; hydrogel; interstitial fluid analysis; livestock; skin perforation

 doi:10.20944/preprints202507.2400.v1

Article

Design of Hydrogel Microneedle Arrays for Interstitial Fluid Analysis and Animal Physiology Monitoring

Laurabelle Gautier [1], Sandra Wiart-Letort [2], Alexandra Massé [3], Caroline Xavier [2], Lorraine Novais-Gameiro [4], Antoine Hoang [1], Marie Escudé [1], Ilaria Sorrentino [1], Muriel Bonnet [3], Florence Gondret [2], Claire Verplanck [1] and Isabelle Texier [1,*]

[1] Université Grenoble Alpes, CEA, LETI-DTBS, Grenoble F-38054, France

[2] PEGASE, INRAE, Institut Agro, Saint-Gilles F-35590, France

[3] INRAE, Université Clermont Auvergne, Vetagro Sup, UMRH, Saint-Genès-Champanelle F-63122, France

[4] Plateforme CICS (Centre Imagerie Cellulaire Santé), Université Clermont Auvergne, F-63000 Clermont-Ferrand, France

* Correspondence: isabelle.texier-nogues@cea.fr; Tel.: +33 438 784 670

Abstract

For monitoring animal adaptation when facing environmental challenges, and more specifically when addressing the impacts of global warming—particularly responses to heat stress and short-term fluctuations in osmotic regulations in the different organs influencing animal physiology—there is an increasing demand for digital tools to understand and monitor a range of biomarkers. Micro-needle arrays (MNAs) have recently emerged as promising devices minimally invasively penetrating human skin to access dermal interstitial fluid (ISF) to monitor deviations in physiology and consequences on health. The ISF is a blood filtrate where the concentrations of ions, low molecular weight metabolites (< 70 kDa), hormones, and drugs, often closely correlate with those in blood. However, anatomical skin differences between human and farm animals, especially large animals, as well as divergent tolerances of such devices among species with behavior specificities, motivate new MNAs design. We addressed technological challenges to design higher microneedles for farm animals (pigs and cattle) measurements. We designed micro-needle arrays composed of 37 microneedles, each 2.8 mm in height, using dextran-methacrylate, a photo-crosslinked biocompatible biopolymer-based hydrogel. The arrays were characterized geometrically and mechanically. Their abilities to perforate pig and cow skin were demonstrated through histological analysis. The MNAs successfully absorbed approximately 10 µL of fluid within 3 hours of application.

Keywords: microneedles; animal health and welfare; hydrogel; interstitial fluid analysis; livestock; skin perforation

1. Introduction

Improving animal adaptation to environmental challenges in order to ensure synergy between production, health, and welfare is widely recognized as a critical component for the sustainability of livestock production systems. It is also essential for addressing ethical and societal demands aimed at reducing antibiotic use and strengthening consumer confidence. Future environmental conditions are expected to become increasingly variable due to the impacts of global warming, amplifying the challenges animals are facing—such as variability in feed nutritional value, water scarcity, heat stress, and increased pathogen pressure. This underscores the urgent need for robust tools to accurately assess animal adaptation, guarantying health and welfare, and inform management decisions that facilitate the adoption of novel practices [1].

 doi:10.20944/preprints202507.2400.v1

Timely, non-invasive, precise, and continuous monitoring of physiological traits is therefore an emerging field in farm animal research to better understand the biological pathways underlying adaptation and to effectively manage animal performance, health, and welfare [2]. Consequently, there is a pressing need for minimally invasive, real-time monitoring of key biomarkers in farm animals. These biomarkers may be proxies of other physiological variables or indicate stress, dehydration, or immune status, and serve as control metrics—such as the quantification of antibiotics or hormones [3–6].

In human medicine, biomarker monitoring via sampling and analysis of interstitial fluid (ISF) has emerged in recent years as a minimally invasive alternative to traditional blood tests [7–10]. The ISF—a plasma filtrate bathing tissues such as the dermis—contains glucose, lactate, electrolytes, and cytokines, with concentrations that can be correlating to those in blood [7,11–13]. Unlike conventional venipuncture, ISF can be accessed using microneedle (MN)-based devices that penetrate the skin with minimal discomfort, enabling continuous, real-time biomarker monitoring over extended periods (hours to days) [7–10,14].

Microneedles (MN)-based devices, comprising microscopic structures designed to locally breach the outer layers of the skin and access the ISF-rich dermal compartment, have predominantly been developed for human applications, with preclinical validation often conducted in rodent and porcine models. More recently, veterinary applications of MN technologies have emerged, especially for transdermal delivery of active compounds [15,16] and vaccines [17,18] across diverse species (dog, pig, guinea pig). Nevertheless, to the extent of our knowledge, only few studies have explored the use of a MN-based device for ISF sampling and analysis in animals [19,20]. Taylor et al. used commercial stainless-steel hollow MNs assembled in a array through a 3D printed piece to puncture rat skin and uptake ISF [20]. Steinbach et al. reported 1.4 mm high stainless-steel solid microneedles coated by calcium-crosslinked alginate hydrogel for ISF sampling of BCG vaccinated cows to assess the animal response to tuberculin [19].

A few fully integrated MN-based devices have been developed for human measurement of key physiological parameters—such as ions and selected metabolites (e.g., glucose)—using optical or electrochemical sensing [21–23]. However, the detection of multiple metabolites, of metabolites requiring more complex analyses (e.g., ELISA), or those present at low concentrations in ISF, demands an alternative approach. In such cases, microneedle arrays (MNAs) can serve primarily as minimally invasive, user-friendly, and painless tools for ISF extraction, which is subsequently subjected to conventional laboratory assays, including liquid chromatography techniques (HPLC, UPLC) or mass spectrometry [8–10,24,25].

Microneedles arrays (MNAs) composed of crosslinked, water-insoluble hydrogels, which initially exhibit high mechanical strength to facilitate skin penetration and rapidly achieve significant swelling within minutes, have been reported to harvest substantial volumes of ISF [24–26]. In human applications, these systems have been utilized for drug monitoring [24,26] and sampling circulating nucleic acids [27]. However, translating this technology to farm (large) animals (e.g., pigs, cattle) presents additional challenges primarily due to their mechanically more resistant skin. Increased skin Young's modulus (e.g., 2.1 MPa for pig dermis/epidermis [28], 83-170 MPa for films of collagen extracted from cattle's skin [29]) in comparison to humans (1.6 MPa for dermis/epidermis [28]) complicates MN insertion without compromising device integrity. Furthermore, longer MNs are required to reach the dermis, given the augmented thickness of the epidermis and stratum corneum layers (e.g., ≈ 55-90 μm for pig [30–32], 600-1400 μm for ear cow [33], in comparison to 50-60 μm for humans ([30,31]) and full skin (e.g., 1.3 (ear)-3.6 (back) mm for pig [30–32], 1.4-3.2 mm for ear cow [33], 3-8 mm for other cow regions [34,35], in comparison to 1.5 mm for human forearm ([30,31]). Hydrogel-based MNAs are typically produced via molding processes, and the manufacture of devices with taller MNs introduces significant challenges, with risks of mechanical failure during demolding. Moreover, tall MNs are more fragile and could easily break or buckle during animal skin insertion.

 doi:10.20944/preprints202507.2400.v1

In this study, we addressed the microfabrication challenges by designing arrays with MNs measuring 2.8 mm in height, fabricated from cross-linked dextran-methacrylate (Dex-MA) hydrogel [36]. These arrays were successfully demonstrated to extract fluid from an in vitro hydrogel model mimicking the skin, and to perforate ex vivo porcine and Holstein cow skin samples.

2. Materials and Methods

2.1. Dextran-Methacrylate (Dex-MA) Synthesis

Dextran-methacrylate with a methacrylate degree of substitution of 32% was synthetized according to previously described protocol [36]. Briefly, dextran T70 (5 g, Mw = 70,000 g/mol, Pharmacosmos (Holbæk, Denmark)) was dissolved in 100 mL of distilled water in a beaker. After complete dissolution, 3.66 ml of methacrylic anhydride (Sigma-Aldrich, Saint-Quentin Fallavier, France) were added dropwise into the polymer solution. The solution was stirred at room temperature (RT) for 1 h. The pH was adjusted using NaOH (3 mol/L) to keep the pH at around 9–11 during the reaction. The obtained Dex-MA solution was dialyzed against distilled water for 1 week (12–14 kDa molecular weight cut-off membrane, Carl Roth, Lauterbourg, France), and lyophilized. The white solid was stored at −20 °C prior to ^{1}H nuclear magnetic resonance (NMR) spectroscopy characterization and use. ^{1}H NMR spectrum in D_2O at 300 MHz, δ (ppm): 2.1 (s, 3H, CH_3-methacrylate), 3.5-4.2 (m, 6H, H-2, H-3, H-4, H-5, H-6, H-6'), 5.1-5.4 (m, 1H, H-1), 5.9 (m, 1H, H-vinyl), 6.5 (m, 1H, H-vinyl).

2.2. Microneedle Array Fabrication

An aluminum master mold featuring the targeted geometry (Figure 1)—an 18 mm diameter microneedle array (MNA) comprising 37 pencil-shaped MNs with a base diameter of 500 µM, each 2800 µm in length, and spaced 1400 µm from tip to tip—was fabricated via precision micromachining. Subsequently, a polydimethylsiloxane (PDMS) mold was produced by casting a degassed PDMS precursor solution with a 10:1 mass ratio of base to crosslinker (Sylgard 184 PDMS kit, Sigma-Aldrich). The cast was cured at 80°C for 3 hours, followed by manual demolding from the aluminum master.

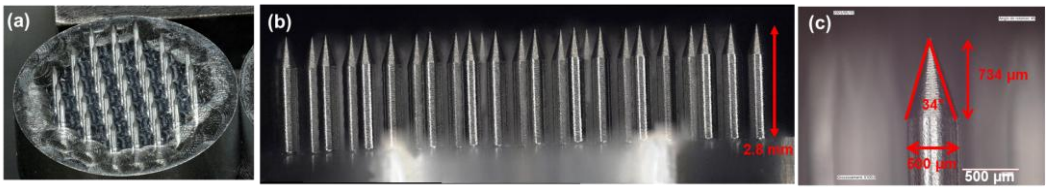

Figure 1. Digital images of the aluminum master featuring the microneedle array (MNA) geometry. (**a**) Overview of the 18 mm diameter MNA with 37 microneedles (MN). (**b**) Side image of the MNA. (**c**) Detail of the geometry of a MN tip.

The polymer solution was prepared in a round-bottom flask covered with aluminum foil, consisting of Milli-Q water containing 20% (w/v) Dex-MA (DS = 32%), 1% (w/v) lithium phenyl-2,4,6-trimethylbenzoylphosphinate (LAP, Sigma-Aldrich, Saint-Quentin Fallavier, France) as photo-initiator, and 5% (w/v) sorbitol (Sigma-Aldrich, Saint-Quentin Fallavier, France) as a humectant. The solution also optionally contained trace amounts of dye (Neutral Red, Brillant Blue) to enhance visualization of the MNs, particularly during phantom and animal skin perforation experiments. The solution was stirred under vacuum for at least 2 hours to ensure homogeneity and degassing. It was then cast into the PDMS mold (associated with the demolding piece), which was mounted on a steel support connected to a vacuum pump. A reduced pressure of 50 mbar was applied for 30 minutes to facilitate complete filling of the MN tips.

 doi:10.20944/preprints202507.2400.v1

The polymer solution was dried within the mold at 35°C for 48 hours. Prior to demolding the MNAs, the Dex-MA hydrogel was crosslinked via photopolymerization by first irradiating the baseplate of the array with 405 nm light (75 mW/cm²) for 5 minutes. Following demolding, the MN side of the patch was subjected to a second 5-minute irradiation under identical conditions to ensure complete crosslinking.

Digital microscopy images of the aluminum master and MNAs were acquired with a Keyence VHX-7000 digital optical microscope in reflectance mode with ring illumination.

2.3. Mechanical Characterization of the Microneedle Arrays

Mechanical testing of the MNAs was performed with a TA.XT Plus texturometer (StableMicrosystems). The MNAs were affixed to a circular probe of 18 mm diameter (matching the MNA size) with the MNs oriented downward. Their mechanical resistance was characterized by uniaxial compression tests against a stainless-steel plate with a maximum compressive load of 49 N (maximum capacity of the device equipped with 5 kg force cell) at a speed of 0.1 mm/s. Following loading, the instrument executed an unloading phase and then returned to its initial position.

2.4. Model Skin Perforation Experiments

SynTissue adult skin (2N) (Syndaver, USA) was used as a commercial model of human skin. SynTissue pieces (cut to 3 x 7 cm dimensions) were set on a custom-designed test bench that allowed to tense the tissue for the perforation assays. Additionally, a rigid backing support was placed beneath the synthetic skin to provide consistent counter-resistance during insertion. An Orbit Inserter (MyLife, Switzerland) was used as an applicator tool to reproducibly insert the MNAs with suitable speed and force into the SynTissue model set on the perforation bench. To attach the MNA to the Orbit Inserter, an adaptor piece was designed and manufactured by 3D printing and the MNA was affixed onto it using double-side tape. After the MNA was applied on the SynTissue, a constant pressure was maintained for 30 seconds before the applicator was removed, and the MNA still attached to the adaptor piece remained into the skin for 2 minutes until removal. The SynTissue and MN devices were then characterized by digital microscopy.

2.5. Model Skin Fluid Uptake Experiments

A 20 mm thick gelatin/agar hydrogel, mimicking dermis, was prepared by mixing 70 g of gelatin (type A, gel strength 300, Sigma-Aldrich), 2.9 g of agar (Sigma-Aldrich) and 10 mg of neutral red dye (to ease visualization), in 290 mL of PBS (phosphate buffer saline, 10 mM phosphate, 137 mM NaCl, 2.7 mM KCl, pH 7.4). The mix was heated in a microwave for 2.5 min at 350 W, energetically stirred with a spatula, and rapidly poured into a 13.6 cm diameter Petri dish. The hydrogel was covered with an aluminum foil to provide a non-humid surface to the skin phantom. The dry MNAs were weighted, then applied onto this skin model using the Orbit Inserter tool, and maintained into the phantom for 15 min, 3h or 24h. After MN device retrieval, MNAs were weighted and observed with a Keyence VHX-7000 digital optical microscope; the gelatin/agar hydrogel was also observed by digital optical microscopy.

2.5. Ex vivo Animal Skin Perforation Experiments

For ex vivo pig experiments, a conventional growing pig (crossbred Pietrain x (Large White x Landrace) weighing about 50 kg (about 80 days of age)), humanely killed after electronarcosis at the experimental slaughterhouse of the UE3P unit (Pig Physiology and Phenotyping Experimental Facility, INRAE, 35 590 St-Gilles, France, 10.15454/1.5573932732039927E12), was used. For cow skin experiments, a Limousine cow (weighing 775 kg, approx. 11 years old) was killed at the experimental slaughterhouse of Herbipôle Research Unit (INRAE, 63 122 Theix, France, 10.15454/1.5572318050509348E12) and desired skin samples were up taken. The perforation

 doi:10.20944/preprints202507.2400.v1

experiments were conducted immediately after the death of the animals, to avoid modifications of skin texture.

The MNAs were applied onto various locations of the animal skin using either the Orbit Inserter applicator or manual thumb pressure. A consistent pressure was maintained for 30 seconds during application. Following insertion, the MNAs remained in place onto the skin for approximately 15-20 minutes for pig experiments, 1 minute for cow experiments, before removal. After application, the MNAs were carefully retrieved and examined using a Keyence VHX-7000 digital optical microscope.

The margins of the tissue to be collected were marked around the MNA application area. A scalpel was then used to carefully excise the surrounding tissue and isolate the sample. The tissue samples were bisected through the center of the MNA application site to allow proper placement into histology cassettes. Immediately after sectioning, the samples were immersed in 4% paraformaldehyde (Thermo Fisher Scientific, Cat. N°: J19943.K2) at room temperature for 4 hours. Following fixation, the samples were stored at 4 °C until transfer to UMR Pegase for pigs, and UMR Herbivores then Centre Imagerie Cellulaire Santé for cattle. Paraffin embedding, microtome sectioning, hematoxylin-eosin (H&E) staining, slide mounting, and microscope imaging were carried out to perform tissue perforation measurements.

3. Results

3.1. MNA Design and Fabrication

Dextran-methacrylate (Dex-MA)-based MNAs were fabricated according to a molding-evaporation process according to classical literature procedures [36], as described in Figure 2a. An aluminum master comprising 37 pencil-shaped microneedles with a center-to-center spacing (pitch) of 1.4 mm, a height of 2.8 mm, and a base diameter of 500 µm was machined and subsequently used to fabricate polydimethylsiloxane (PDMS) negative molds.

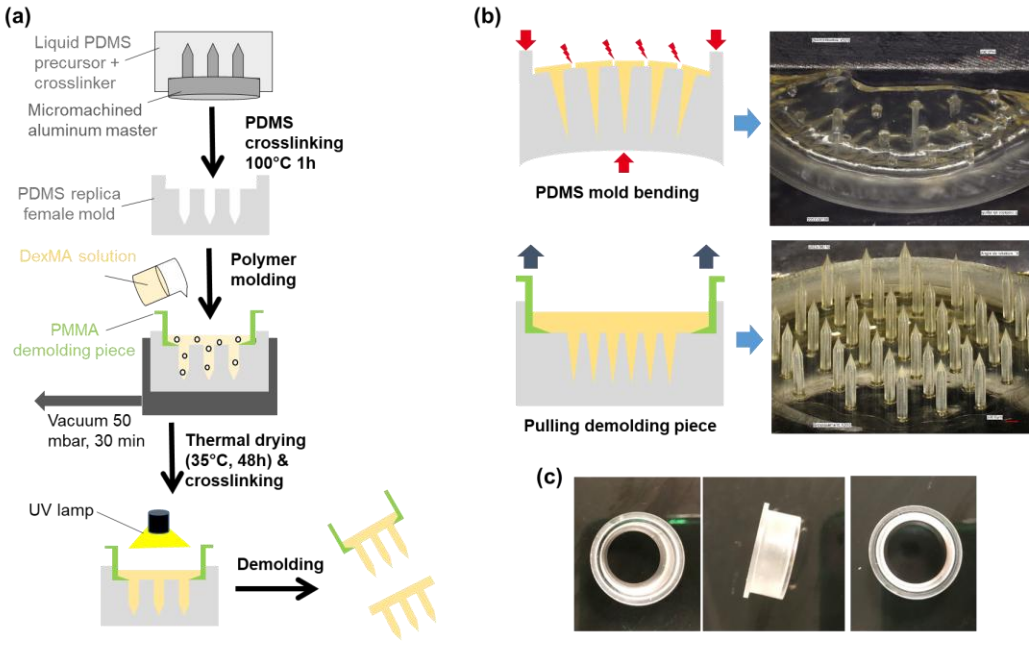

Figure 2. Fabrication of dextran-methacrylate (Dex-MA) MNAs with high MNs. (**a**) Schematic flow of the fabrication process with the preparation of the polydimethylsiloxane (PDMS) mold, polymer molding, drying, UV crosslinking and demolding. (**b**) Details of the demolding step without (top images) and with (bottom images) a poly(methyl methacrylate) (PMMA) demolding piece. (**c**) Photographs of the PMMA demolding piece.

The Dex-MA solution was then poured into the molds that were filled till the MN tips with the aid of vacuum. The polymer solution was thermally dried, and UV-crosslinking of methacrylate groups was performed by irradiating the top of the device. After demolding, UV-crosslinking was

 doi:10.20944/preprints202507.2400.v1

also performed on the MN tip side. However, two challenges were encountered in the fabrication of these high MN devices (2.8 mm height MN) that were not previously observed for shorter ones (< 1200 μm) [36].

First, the demolding step could not be performed efficiently with high MN arrays. As displayed in Figure 2b, bending the PDMS mold was shown to be ineffective since causing damages to both the array baseplate and the MNs because of the high mechanical constraints. Therefore, a poly(methyl methacrylate) (PMMA) demolding piece was designed and fabricated by machining (Figure 2c). It allowed for vertical pulling of the dried MNAs that could be easily demolded without breaking.

Secondly, the MNAs obtained initially based on a polymer solution containing only Dex-MA at 20% w/v and the LAP photo-initiator at 1% w/v in distillated water presented several defects. While the basis of all microneedles could be present on the array after demolding, the majority of the device MNs contained internal bubbles that could induce MN fragility and eventually breaking. Moreover, the baseplate of the MNAs was extensively cracked, rendering the devices unusable. Such defects could originate from poor mold filling process, insufficient quantity of polymer or excessive solution viscosity, or inappropriate water evaporation during drying. Different optimization assays revealed the issue stemmed from the drying phase. Consequently, drying parameters were modified based on the premise that the previous drying protocol (24 hours at 40°C followed by 24 hours at 80°C) induced excessive drying rates, likely causing rapid water evaporation, material shrinkage, and subsequent cracking and bubble formation. The drying regime was altered to a single-stage drying for 48 hours at 35°C but with only partial improvement in MNA quality, which continued to exhibit significant bubble formation within the microneedles and cracking of the baseplate (Figure 3a). To achieve controlled drying while maintaining reasonable processing times, the incorporation of a humectant additive was therefore proposed. Sorbitol and glycerol, commonly used humectants in pharmaceutical and food formulations, were selected for evaluation based on concentrations reported in the literature [37–39]. Formulations containing glycerol did not yield conclusive improvements. In contrast, MNAs prepared with Dex-MA formulations containing 5% w/v sorbitol exhibited baseplates free of cracks and MNs devoid of bubbles (Figure 3b).

The MNAs obtained with this optimized process were geometrically characterized using digital microscopy, and demonstrated reproducible and satisfactory fidelity to the aluminum master mold, with in particular a microneedle height of 2661 ± 15 μm (> 95% of targeted value).

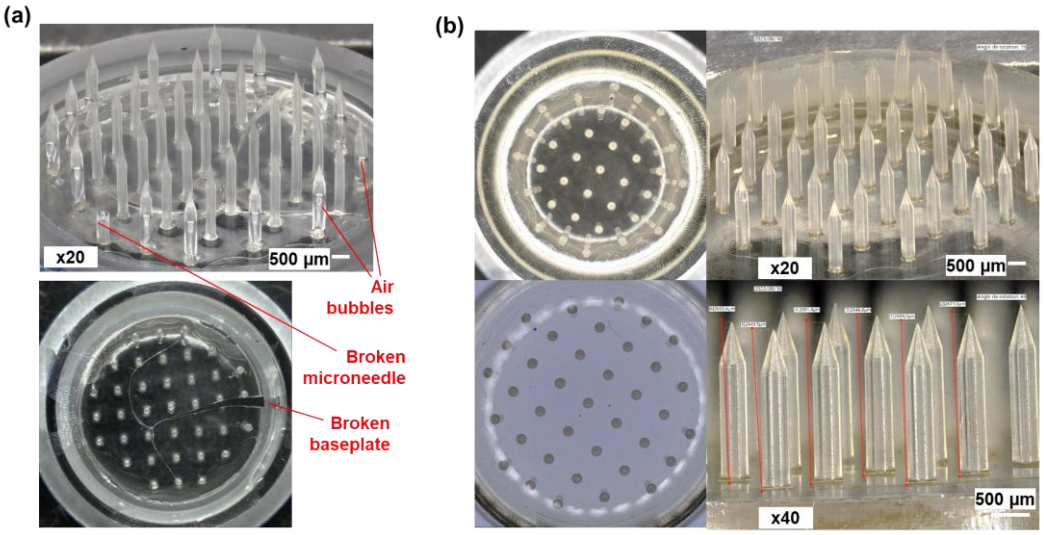

Figure 3. Optimization of the polymer formulation for the fabrication of Dex-MA MNAs with high microneedles. (**a**) Molding of MNAs using Dex-MA/LAP formulation (Dex-MA 20% w/v, LAP 1% w/v, in distillated water). (**b**) Molding of MNAs using Dex-MA/LAP/sorbitol formulation (Dex-MA 20% w/v, LAP 1% w/v, sorbitol 5% w/v, in distillated water).

 doi:10.20944/preprints202507.2400.v1

3.2. MNA Mechanical Characterization

To evaluate the mechanical properties of the Dex-MA MNAs, compression tests were conducted against a stainless-steel plate with a maximum compressive load of 49 N (Figure 4a). The photographs of the devices before and after compression (Figure 4b) showed that all microneedles were present after compression, and structurally unbroken, as also evidenced by the continuous loading and unloading curves recorded by the texturometer that did not show disruption, therefore indicating no MN break (Figure 4c). This result suggested that each microneedle could withstand an applied force of approximately 1.3 N without failure. Only a slight deformation at the MN tips could be observed. Importantly, no MN buckling was evidenced, demonstrating the mechanical resistance of the dried polymer material.

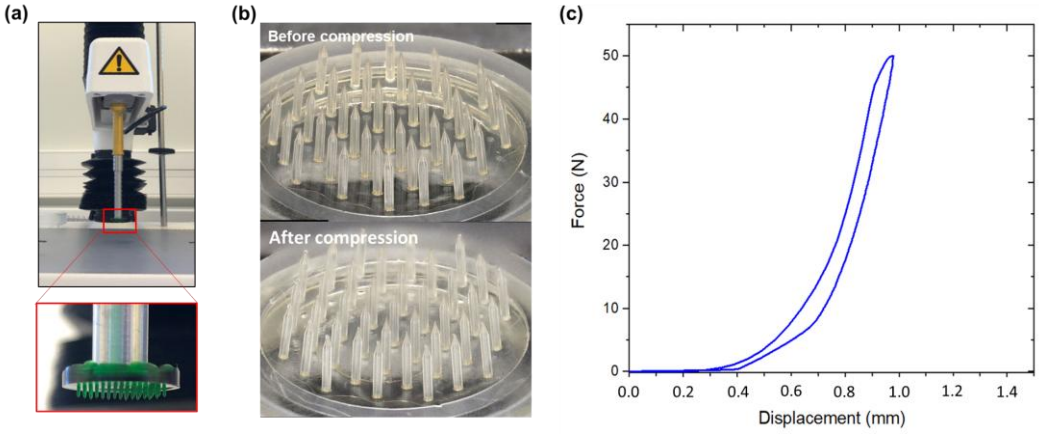

Figure 4. Mechanical characterization of Dex-MA MNAs with high microneedles. (**a**) Photograph of the experiment test with the MNA attached to the texturometer probe being compressed onto a steel plate. (**b**) Digital microscope images of a MNA before and after compression. (**c**) Force=f(displacement) curve during loading and unloading.

3.3. Development of Perforation Protocol on Human Skin Model

A perforation protocol was developed using SynTissue as a commercial human skin phantom and a slightly modified commercial Orbit Inserter applicator (Figure 5a), through the use of a dedicated bench that allowed to pre-tense the synthetic tissue (Figure 5b). After application of the MNAs on the SynTissue, a constant pressure was maintained for 30 seconds before the applicator was removed, in order to favor reproducible tissue perforation and not only deformation. The MNAs still attached to the adaptor piece were remained into the artificial skin for 2 additional minutes before being removed. The MNAs were then inspected post-perforation to identify any structural damage incurred during insertion (Figure 5c). The integrity of the Dex-MA MN devices was maintained post-perforation, with all microneedles intact and free from fracture. However, a shear band oriented at approximately 45°—denoted by the white dotted lines in Figure 5c—was occasionally observed in some microneedles following the perforation test, although no material failure occurred along this band. Furthermore, the 37 perforations pattern generated by the MNs into the skin phantom was clearly visible after array insertion (Figure 5d), indicating a 100% perforation rate across all needles. This experiment was replicated multiple times, yielding highly consistent and reproducible outcomes. Collectively, these results confirm the high efficacy of the devices in perforating synthetic human skin phantoms using the developed application protocol.

 doi:10.20944/preprints202507.2400.v1

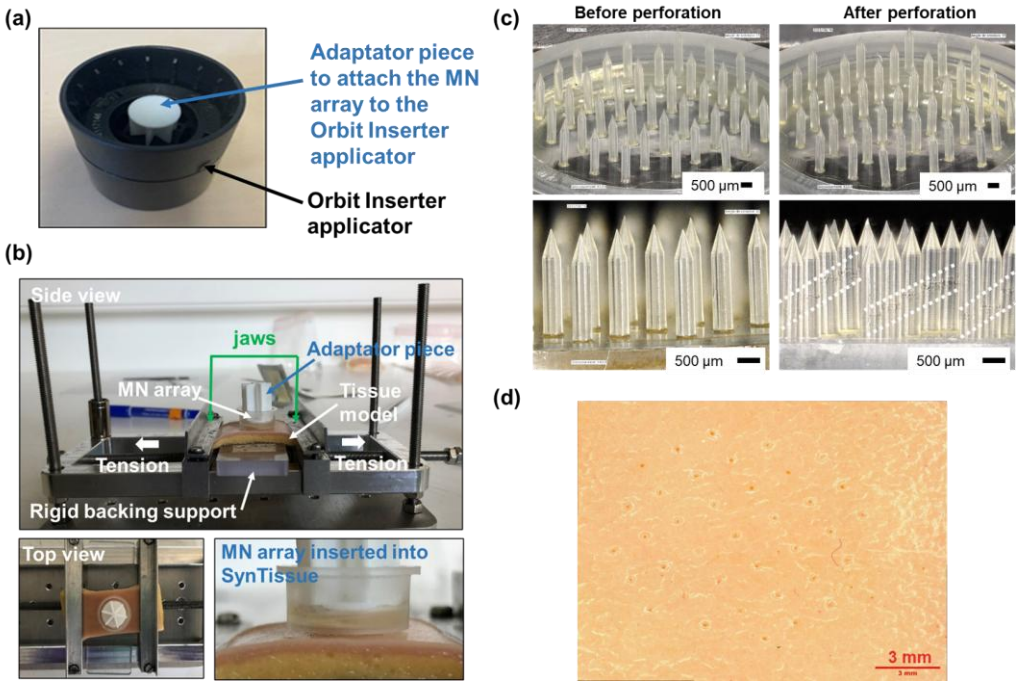

Figure 5. Perforation of human skin model. (**a**) Photograph of the Orbit Inserter assembled with the adaptation piece to attach the MNA. (**b**) Photographs of the perforation bench mounted with SynTissue after application of a MNA. (**c**). Digital microscopy images of a Dex-MA MNA before and after 2 minutes insertion in SynTissue. (**d**) Digital microscopy image of SynTissue after the insertion of a Dex-MA MNA.

3.4. Fluid Uptake Experiments on Model Skin

SynTissue, a textile impregnated with a water/ethanol preservative solution and featuring a persistently moist surface, does not replicate the water content of biological skin and is therefore unsuitable for fluid uptake studies. To better assess the ISF uptake capacity of the MNAs, we employed a gelatin/agar hydrogel containing approximately 75% water, as a tissue-mimicking model. To provide a dry interface with the MN device, the hydrogel surface was covered with an aluminum foil (Figure 6a). Dex-MA MNAs were weighed prior to application, then inserted into the skin phantom using the Orbit Inserter applicator. The arrays remained in place for durations of 15 minutes, 3 hours, and 24 hours, before careful removal. Post-insertion, the gelatin/agar hydrogels were examined via digital microscopy, revealing a distinct pattern of 37 MN perforations (Figure 6b). The MNAs were reweighed following removal, and the difference in mass before and after insertion was used to quantify the amount of fluid absorbed during the application period (Table 1). The inclusion of a dye in the hydrogel matrix enabled visual tracking of fluid diffusion into the MN tips, providing qualitative confirmation of uptake (Figures 6c–e; Table 1). We observed a time-dependent increase in both the volume of absorbed fluid and the extent of dye penetration into the MN tips, reaching a maximum uptake of 31.4 mg after 24 hours. Notably, the fluid diffused along approximately 70% of the MN length, regardless of insertion duration. To note that after 24 hours application, some MNs were broken after removal of the device from the skin phantom.

 doi:10.20944/preprints202507.2400.v1

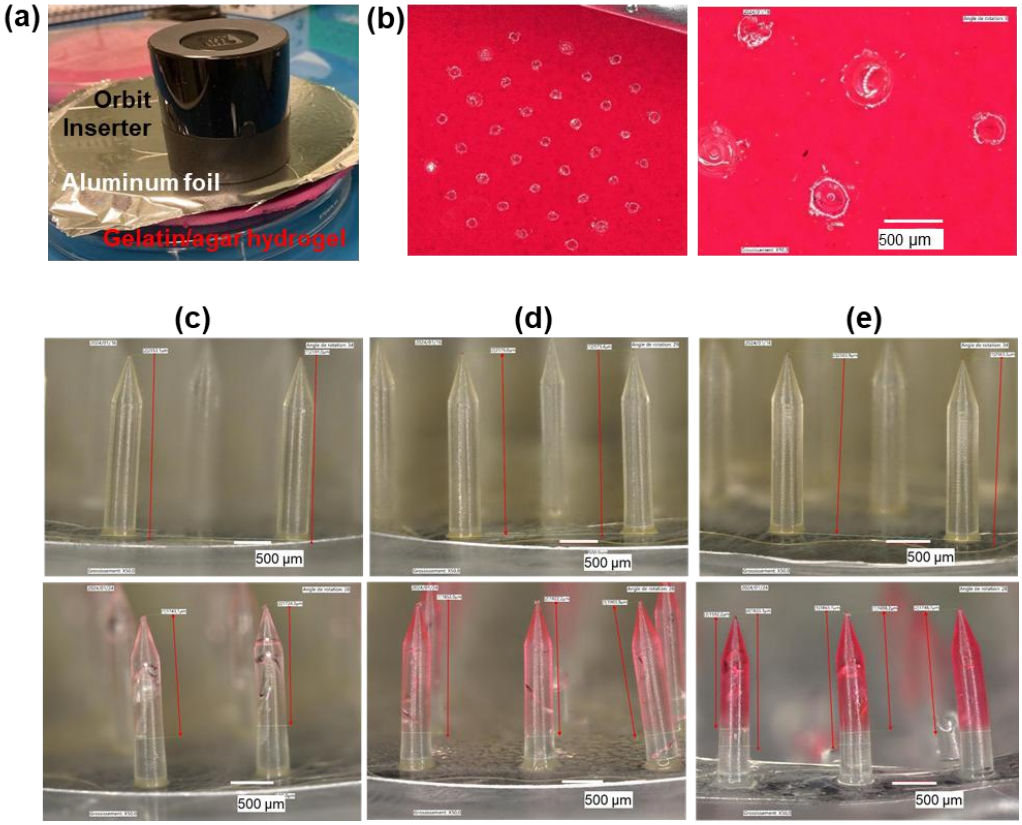

Figure 6. Fluid uptake in gelatin/agar hydrogel model. (**a**) Photograph of the insertion of a MNA into the skin phantom with the use of the Orbit Inserter. (**b**) Digital microscopy images of the gelatin/agar hydrogel after 15 min application of a MNA. (**c, d, e**) Digital microscopy images of the MNAs before (top) and after (bottom) insertion into and retrieval from the gelatin/agar hydrogel after 15 minutes (**c**), 3 hours (**d**), and 24 hours (**e**) of application.

Table 1. Fluid diffusion from the gelatin/agar hydrogel to the MNA.

Duration of MNA insertion	**Amount of up taken fluid (mg)**	**Length of MN tip into which the liquid has diffused (µm)** *(% of the MN total height)*
15 min	ND[1]	1665 *(65%)*
3 h	10.7	1908 *(75%)*
24 h	31.4	1579 *(62%)*

[1] ND: not measurable.

3.5. Porcine Skin Perforation Experiments

Porcine skin perforation experiments were conducted on the euthanized animal. Dex-MA MNAs were applied using the Orbit Inserter at various anatomical sites (Figure 7a): the right side of the neck behind the ear (1), lower (2) and upper (4) regions of the neck, the lateral side of the right forelimb (3), the chest between the forelimbs (5), and the inner surface of the ear (6). No structural damage to the MNAs was observed either during insertion or upon removal of the devices (Figure 7b).

The MNAs achieved successful skin perforation in most regions, including the neck, shoulder, forelimb, and chest (Figure 7c), but failed to penetrate the skin of the inner ear (region 6). Histological analysis (Figure 7d) revealed penetration depths between approximately 200 and 1000 µm, with the MNs effectively breaching the stratum corneum and reaching the dermal layer.

 doi:10.20944/preprints202507.2400.v1

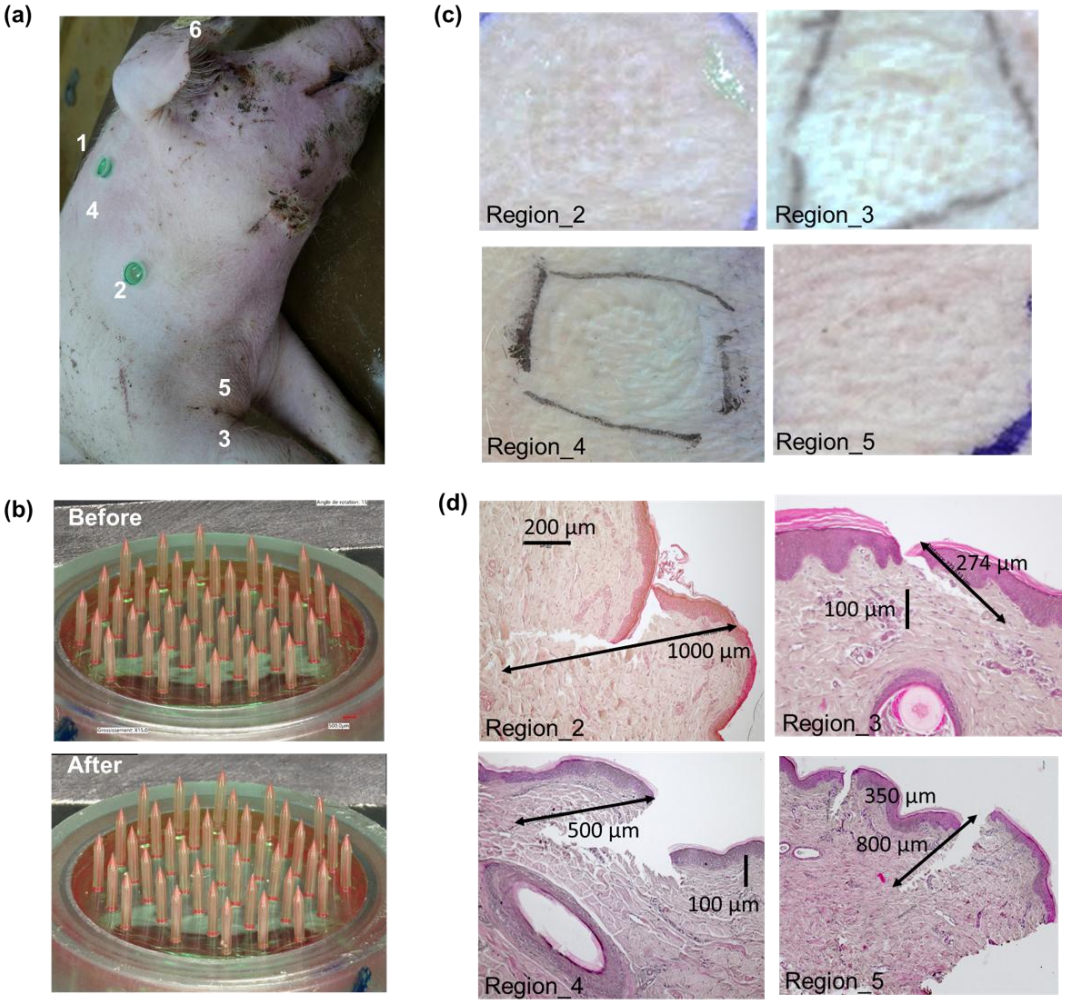

Figure 7. Porcine skin perforation experiments. (**a**) Photograph of the animal and the different regions where perforation was tested: right side of the neck behind the ear (1), lower part of the neck (2), external part of the right forelimb (3), higher part of the neck (4), chest between the two forelimbs (5), and inner surface of the ear (6). (**b**) Digital microscopy images of a MNA before and after insertion. (**c**) Photographs of different regions of skin after MNA removal. (**d**) Histology images of skin samples collected from different regions after MNA insertion.

3.6. Cow Skin Perforation Experiments

Ex vivo skin perforation experiments were conducted on freshly excised cow ear and neck tissues obtained immediately post-euthanasia. Complete insertion of the MNAs using the Orbit Inserter (Figure 8a) was not achieved in either the ear nor the neck tissue. Consequently, successful insertion was accomplished manually via thumb pressure, accompanied by the application of a counter-force (Figure 8b–d). Nevertheless, device adhesion to the ear tissue was suboptimal, whereas the neck region demonstrated qualitatively superior compatibility in terms of both insertion facility and device retention.

Histological analysis of both tissue types confirmed successful MN penetration through the stratum corneum into the dermal layer (Figure 8e–f). Although additional studies are warranted to reinforce these findings, preliminary observations suggest that MN perforation in the neck tissue was generally deeper (436 ± 295 µm) than in the ear (314 ± 120 µm).

 doi:10.20944/preprints202507.2400.v1

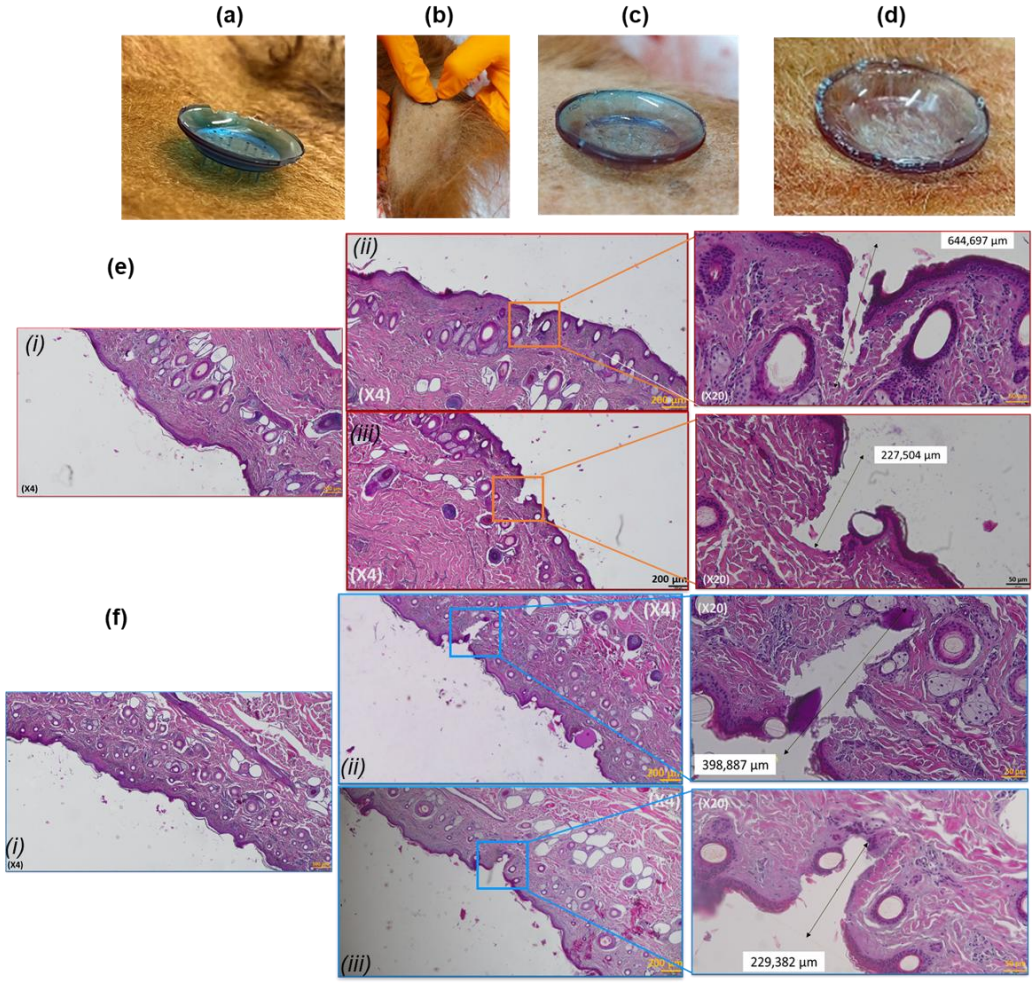

Figure 8. Cow skin perforation experiments. (**a**) Photograph of a MNA applied with the Orbit Inserter applicator on cow's neck tissue. (**b**) Photograph of the application of a MNA on cow's ear tissue by thumb pressure by exerting a counter-push. (**c**, **d**) Photographs of MNAs applied by thumb pressure on cow's external ear (**c**) and neck (**d**) tissues. (**e**, **f**) Histology images of cow's external ear (**e**) and neck (**f**) tissues: (i) non-perforated tissue region; (ii, iii): perforated tissue regions at x4 (left) and x20 (right) magnifications.

4. Discussion

4.1. Hydrogel-Based MNA for ISF Uptake

Real-time, minimally invasive monitoring of physiological biomarkers is critical for effective assessment and management of animal performance, health, and welfare, and more importantly, using wearable devices allowing continuous measurements without restraining the animals. This necessitates the development of advanced analytical tools. In human medicine, microneedle arrays have been recognized for their ability to enable painless extraction of dermal interstitial fluid (ISF), a biofluid rich in clinically relevant biomarkers [8,10,11,40]. For applications involving global biomarker profiling or discovery of multi-analyte signatures, ISF sampling followed by advanced analytical techniques—particularly omics-based approaches—represents a promising strategy.

Chemically crosslinked hydrogel-based MNAs are particularly well-suited for this purpose. These hydrogels form three-dimensional polymer networks capable of absorbing large volumes of aqueous fluid without dissolving, thereby maintaining their structural integrity. When dried and molded into MN structures, they possess sufficient mechanical strength to perforate the skin and rapidly absorb ISF upon contact with the dermal compartment [24–26].

In this study, we selected photo-crosslinked dextran-methacrylate (Dex-MA) as the material of choice for MNA fabrication. In previous work, we systematically evaluated the mechanical and

 doi:10.20944/preprints202507.2400.v1

swelling properties of Dex-MA synthesized from dextran with varying molecular weights and degrees of methacrylate substitution (DS) [36]. We identified Dex-MA derived from dextran of 70,000 g/mol molecular weight and a DS of 32% as an optimal formulation for a MNA dedicated to ISF uptake [41]. This formulation demonstrated a favorable balance between swelling capacity (approximately 50%) and mechanical toughness in the dry state, with a Young's modulus of 2.5–3 MPa [36]. This modulus exceeds that of porcine skin (approximately 2.1 MPa for dermis/epidermis [28]), suggesting sufficient rigidity for tissue penetration. In the present study, dried photo-crosslinked Dex-MA material, when shaped into a microneedle array, withstood compressive forces up to 50 N against a steel plate without exhibiting needle fracture or buckling. Previous literature reports insertion forces ranging from a few Newtons up to 30 N in human or porcine skin [42–44], suggesting once again sufficient mechanical resistance to perforate porcine skin.

While specific data for cattle skin are lacking, reported Young's modulus values for films derived from bovine skin collagen range from 83 to 170 MPa [29]; however, these values could be far above those of native tissue properties. It is also important to note that Young's modulus represents only one aspect of the skin complex mechanical behavior, which is highly viscoelastic and varies depending on anatomical location.

4.2. MNA Design

As with mechanical properties, skin thickness varies markedly across body regions. Therefore, the anatomical site of application significantly influences MNA design, particularly with respect to microneedle height. For example, Simon et al. reported bovine ear skin thickness ranging from 1000 to 1400 μm, depending on the specific area (e.g., apex, base, or top of the pinna) [33], while other anatomical regions in cattle exhibit skin thicknesses between 3 and 8 mm [34,35]. In pigs, skin thickness ranges from approximately 1.3 mm in the ear to 3.6 mm on the back [30–32].

The ear presents a seemingly attractive site for MNA application in cattle, given its current use for identification tagging. However, its high cartilage content may hinder effective skin perforation and the ISF (hydration) content of this tissue is unknown. Alternatively, the neck may offer a more suitable site due to its relatively homogeneous tissue composition and accessibility; it also allows for secure post-application strapping to stabilize the device. In pigs, auricular sites are not ideal due to social behaviors of the animals when reared in collective pens, particularly ear-biting and fighting, which could compromise device integrity and longevity. Accordingly, alternative locations such as the back, abdomen, or neck should be explored, despite their relatively greater skin thickness.

Considering interspecies and inter-individual variations, as well as the variability in skin properties across anatomical sites, we designed MNAs with a microneedle height of 2.8 mm. This dimension was selected based on available histological data for porcine and bovine skin [30–33], and with the aim of ensuring consistent dermal penetration and reliable ISF access across diverse tissue types and breeds. Notably, we considered that using arrays presenting tall MNs would offer the most practical and reliable option for conducting animal experiments across different anatomical sites, both in pig and cow.

4.3. MNA Fabrication

Fabricating MNAs with 2.8 mm height microneedles and a tip-to-tip spacing of 1400 μm poses considerable technical challenges, particularly during the demolding step, which is highly dependent on array geometry. As MN height and density increase, perpendicular removal from the mold becomes essential. For arrays with MNs 800–1400 μm in height, gentle mold flexing typically suffices to release the array intact. However, for taller MNs as developed here, mold bending caused basal plate fragmentation and MN detachment, rendering the devices nonfunctional. To address this, a custom PMMA demolding insert, matching the 18 mm diameter mold, was fabricated and positioned beneath the hydrogel during casting. It facilitated vertical extraction of the patch, preserving structural integrity.

 doi:10.20944/preprints202507.2400.v1

Initial arrays made from Dex-MA/LAP formulation exhibited internal bubbles and severe baseplate cracking, compromising device quality. Attempts to slow drying by adjusting process parameters were ineffective. To address this, a humectant—sorbitol, widely used in pharmaceutical and food formulations [38,39]—was incorporated to retain water and control drying kinetics. Sorbitol significantly reduced cracking and bubble formation, demonstrating its potential to improve mechanical robustness during MNA fabrication.

These protocol enhancements enabled the successful fabrication of MNAs with 2.8 mm-high MNs—the tallest hydrogel-based microneedles reported to date, to the best of our knowledge.

4.4. MNA Skin Perforation

With the tall MNAs fabricated via a reliable and reproducible process in hand, we next focused on developing a robust and consistent perforation protocol. The insertion force and application speed of a MNA are critical parameters for efficient skin penetration [43]. To deliver a precisely controlled impact, we selected a commercial Orbit Inserter applicator and engineered an adaptor to securely mount the MNAs onto this platform.

The application protocol was initially optimized using a synthetic skin model, SynTissue, which mimics the dermis (1 mm thickness) and hypodermis (3 mm thickness) layers of human skin, and is typically employed for surgical incision and suture training. Additionally, a custom-designed test bench was utilized to pre-tension the tissue, simulating in vivo conditions. Under these conditions, we achieved 100% perforation efficacy with the MNAs, and the MNs withstood the mechanical stresses of insertion, although early signs of material microfractures were observed in some needles.

Subsequently, ex vivo perforation studies were performed on freshly excised porcine and bovine tissues obtained immediately post-euthanasia. Multiple anatomical sites (ear, neck, shoulder, forelimb, and chest) were assessed for porcine skin perforation. Successful perforation was achieved at all sites except the ear, which we attribute to the underlying cartilage beneath the thin skin layer, complicating patch adhesion. Furthermore, the natural social behaviors of pigs render ear application challenging in practical settings. For bovine tissue, ear and neck sites were tested; however, the Orbit Inserter was ineffective in delivering the MNAs into these tissues. Moreover, partial or complete device breakage could occur during application. Consequently, manual application by thumb pressure with counterforce applied to the opposite side of the tissue was employed, providing a less reproducible but more adaptable method to ensure perforation. Although the ear was initially considered an optimal site and histology confirmed successful perforation, the neck emerged as a more practical and comfortable location, consistent with observations in porcine skin.

It is established that MNs typically penetrate approximately 60% of their length into human skin during insertion [45]. In gelatin/agar phantoms, we observed MN penetration depths of approximately 60–75% of their length (1600–1900 μm). However, histological analysis revealed substantially lower perforation depths in porcine skin (275–1000 μm) and bovine skin (225-645 μm). This discrepancy may reflect reduced penetration efficiency due to intrinsic differences in animal skin properties relative to human, as well as partial tissue collapse during histological processing, complicating accurate quantification. Additionally, prior studies have demonstrated that rigor mortis rapidly develops post-euthanasia, leading to increased porcine skin stiffness that diminishes MNA penetration depth compared to living tissue [46]. Therefore, the perforation efficiencies measured ex vivo likely underestimate those achievable in vivo.

Nevertheless, these preliminary results demonstrate the capability of Dex-MA-based MNAs to perforate both porcine and bovine skin, validating their potential for further in vivo investigation.

4.4. MNA Fluid Uptake

To assess the fluid absorption capacity of the MNAs under controlled conditions, swelling studies were conducted using a synthetic gelatin/agar phantom, which possesses approximately 80% water content—comparable to the 70–75% water content reported for porcine skin [47]. In this model, fluid uptake by the hydrogel MNs was evident, with absorption reaching 10.7 μL after 3 hours and

 doi:10.20944/preprints202507.2400.v1

up to 31.4 µL after 24 hours. Although fluid uptake could not be quantified gravimetrically after 15 minutes of insertion into the phantom, slight diffusion of a dye previously incorporated into the hydrogel was observed visually, suggesting limited but detectable absorption. This limited uptake may be attributed to the swelling kinetics of Dex-MA hydrogels, which typically reach equilibrium within 1–2 hours when fully immersed in saline solution [36].

These preliminary findings indicate that Dex-MA microneedle arrays are capable of absorbing interstitial fluid upon insertion, and suggest that a minimum application time of several hours may be required to achieve appreciable fluid uptake in vivo.

5. Conclusions

This study demonstrates the feasibility of using photo-crosslinked Dex-MA hydrogel-based MNAs to perforate the skin and give access to interstitial fluid in large animal models, specifically pigs and cattle.

We successfully developed a robust and reproducible fabrication protocol yielding MNAs with 2.8 mm-tall MNs—the tallest hydrogel-based structures of their kind reported to date, to our knowledge. Ex vivo investigations using porcine and bovine tissues showed the capability of the MNAs to perforate multiple anatomical sites effectively. Additionally, fluid absorption assays performed with a skin-mimicking hydrogel demonstrated that the MNAs could uptake between 10 and 30 µL of fluid within a few hours.

The experimental methodology was designed to closely replicate realistic application conditions, thereby laying the groundwork for subsequent in vivo studies. The results indicate that an application duration of several hours is required to achieve meaningful fluid uptake in the order of tens of microliters, and identified the neck as a particularly suitable anatomical site for secure and sustained MNA placement. Building upon these findings, future in vivo experiments are planned to refine application protocols, evaluate interstitial fluid uptake efficacy under physiological conditions, and facilitate translation to practical field deployment.

Overall, this work provides a critical step toward the development of advanced biosampling technologies for animal health monitoring, with potential applications in precision livestock farming and veterinary diagnostics.

Author Contributions: Conceptualization, L.G., F.G. and I.T.; methodology, L.G., A.H., S.W.L., A.M., M.B., I.T.; investigation, L.G., A.H., S.W.L., A.M., C.X., L.N.G., M.E., and F.G.; resources, L.G., A.H., A.M., C.X., M.E., and C.V.; writing—original draft, L.G. and I.T.; writing—review and editing, L.G., A.H., S.W.L., A.M., C.X., L.N.G., M.E., I.S., M.B., F.G., C.V. and I.T.; visualization, L.G., S.W.L., A.M., and I.T.; supervision, I.S., M.B., F.G., C.V. and I.T.; project administration, M.B., F.G., and C.V.; funding acquisition, M.B. and F.G. All authors have read and agreed to the published version of the manuscript.

Funding: This research was funded by Agence Nationale de la Recherche under the France 2030 program under the reference ANR-22-PEAE-0008.

Data Availability Statement: The raw data supporting the conclusions of this article will be made available by the authors on request.

Acknowledgments: We acknowledge the French National Research Agency in the framework of the France 2030 program (ANR-22-PEAE-0008) under the WAIT4 project for funding. The authors thank the staff of the INRAE Herpipôle Research Unit (UE1414, Theix, France; doi.org/10.15454/1.5572318050509348E12) for their valuable assistance in setting up the cow experiments, and Cécile Coudy-Gandilhon (UNH, UMR 1019, INRAE, Theix, France) for her technical support with the histological analyses. LETI-DTIS is supported by the French National Research Agency in the framework of the Labex Arcane, CBH-EUR-GS program (ANR-17-EURE-003) and Glyco@Alps "Investissement d'Avenir" program (ANR-15-IDEX-02).

Conflicts of Interest: The authors declare no conflicts of interest.

 doi:10.20944/preprints202507.2400.v1

References

1. Pérez, S.; Calvo, J.H.; Calvete, C.; Joy, M.; Lobón, S. Mitigation and Animal Response to Water Stress in Small Ruminants. *Anim. Front.* **2023**, *13*, 81–88, doi:10.1093/af/vfad049.
2. Sorrentino, I.; Verplanck, C.; Thomas, Y.R.J. Electrochemical Sensors for Animal Welfare. In Proceedings of the Eurosensors 2023; MDPI, March 18 2024; p. 45.
3. Babington, S.; Tilbrook, A.J.; Maloney, S.K.; Fernandes, J.N.; Crowley, T.M.; Ding, L.; Fox, A.H.; Zhang, S.; Kho, E.A.; Cozzolino, D.; et al. Finding Biomarkers of Experience in Animals. *J. Anim. Sci. Biotechnol.* **2024**, *15*, doi:10.1186/s40104-023-00989-z.
4. Marco-Ramell, A.; De Almeida, A.M.; Cristobal, S.; Rodrigues, P.; Roncada, P.; Bassols, A. Proteomics and the Search for Welfare and Stress Biomarkers in Animal Production in the One-Health Context. *Mol. Biosyst.* **2016**, *12*, 2024–2035, doi:10.1039/c5mb00788g.
5. Whelan, R.; Tönges, S.; Böhl, F.; Lyko, F. Epigenetic Biomarkers for Animal Welfare Monitoring. *Front. Vet. Sci.* **2023**, *9*, doi:10.3389/fvets.2022.1107843.
6. Zachut, M.; Šperanda, M.; De Almeida, A.M.; Gabai, G.; Mobasheri, A.; Hernández-Castellano, L.E. Biomarkers of Fitness and Welfare in Dairy Cattle: Healthy Productivity. *J. Dairy Res.* **2020**, *87*, 4–13, doi:10.1017/s0022029920000084.
7. Madden, J.; O'Mahony, C.; Thompson, M.; O'Riordan, A.; Galvin, P. Biosensing in Dermal Interstitial Fluid Using Microneedle Based Electrochemical Devices. *Sens. Bio-Sens. Res.* **2020**, *29*, 100348, doi:10.1016/j.sbsr.2020.100348.
8. Kashaninejad, N.; Munaz, A.; Moghadas, H.; Yadav, S.; Umer, M.; Nguyen, N.-T. Microneedle Arrays for Sampling and Sensing Skin Interstitial Fluid. *Chemosensors* **2021**, *9*, 83, doi:10.3390/chemosensors9040083.
9. Lu, H.; Zada, S.; Yang, L.; Dong, H. Microneedle-Based Device for Biological Analysis. *Front. Bioeng. Biotechnol.* **2022**, *10*, doi:10.3389/fbioe.2022.851134.
10. Liu, G.-S.; Kong, Y.; Wang, Y.; Luo, Y.; Fan, X.; Xie, X.; Yang, B.-R.; Wu, M.X. Microneedles for Transdermal Diagnostics: Recent Advances and New Horizons. *Biomaterials* **2020**, *232*, 119740, doi:10.1016/j.biomaterials.2019.119740.
11. Wu, Z.; Qiao, Z.; Chen, S.; Fan, S.; Liu, Y.; Qi, J.; Lim, C.T. Interstitial Fluid-Based Wearable Biosensors for Minimally Invasive Healthcare and Biomedical Applications. *Commun. Mater.* **2024**, *5*, doi:10.1038/s43246-024-00468-6.
12. Oharazawa, A.; Maimaituxun, G.; Watanabe, K.; Nishiyasu, T.; Fujii, N. Metabolome Analyses of Skin Dialysate: Insights into Skin Interstitial Fluid Biomarkers. *J. Dermatol. Sci.* **2024**, *114*, 141–147, doi:10.1016/j.jdermsci.2024.04.001.
13. Friedel, M.; Thompson, I.A.P.; Kasting, G.; Polsky, R.; Cunningham, D.; Soh, H.T.; Heikenfeld, J. Opportunities and Challenges in the Diagnostic Utility of Dermal Interstitial Fluid. *Nat. Biomed. Eng.* **2023**, *7*, 1541–1555, doi:10.1038/s41551-022-00998-9.
14. Himawan, A.; Vora, L.K.; Permana, A.D.; Sudir, S.; Nurdin, A.R.; Nislawati, R.; Hasyim, R.; Scott, C.J.; Donnelly, R.F. Where Microneedle Meets Biomarkers: Futuristic Application for Diagnosing and Monitoring Localized External Organ Diseases. *Adv. Healthc. Mater.* **2023**, *12*, doi:10.1002/adhm.202202066.
15. Miranda-Muñoz, K.; Midkiff, K.; Woessner, A.; Afshar-Mohajer, M.; Zou, M.; Pollock, E.; Gonzalez-Nino, D.; Prinz, G.; Hutchinson, L.; Li, R.; et al. A Multicomponent Microneedle Patch for the Delivery of Meloxicam for Veterinary Applications. *ACS Nano* **2024**, *18*, 25716–25739, doi:10.1021/acsnano.4c08072.
16. Yang, Y.; Deng, X.; Chen, Z.; Lin, X.; Hu, Y.; Zeng, Q.; Wang, D.; Guo, P.; Yin, G.; Wang, L. Dissolving Cinnamaldehyde HA/PVA Microneedles for the Treatment of Skin Diseases Caused by Microsporum Canis. *J. Drug Deliv. Sci. Technol.* **2025**, *107*, 106841, doi:10.1016/j.jddst.2025.106841.
17. Vreman, S.; Stockhofe-Zurwieden, N.; Popma-de Graaf, D.J.; Savelkoul, H.F.J.; Barnier-Quer, C.; Collin, N.; Collins, D.; McDaid, D.; Moore, A.C.; Rebel, J.M.J. Immune Responses Induced by Inactivated Porcine Reproductive and Respiratory Syndrome Virus (PRRSV) Vaccine in Neonatal Pigs Using Different Adjuvants. *Vet. Immunol. Immunopathol.* **2021**, *232*, 110170, doi:10.1016/j.vetimm.2020.110170.
18. Choi, I.-J.; Na, W.; Kang, A.; Ahn, M.-H.; Yeom, M.; Kim, H.-O.; Lim, J.-W.; Choi, S.-O.; Baek, S.-K.; Song, D.; et al. Patchless Administration of Canine Influenza Vaccine on Dog's Ear Using Insertion-Responsive

 doi:10.20944/preprints202507.2400.v1

Microneedles (IRMN) without Removal of Hair and Its in Vivo Efficacy Evaluation. *Eur. J. Pharm. Biopharm.* **2020**, *153*, 150–157, doi:10.1016/j.ejpb.2020.06.006.

19. Steinbach, S.; Jalili-Firoozinezhad, S.; Srinivasan, S.; Melo, M.B.; Middleton, S.; Konold, T.; Coad, M.; Hammond, P.T.; Irvine, D.J.; Vordermeier, M.; et al. Temporal Dynamics of Intradermal Cytokine Response to Tuberculin in Mycobacterium Bovis BCG-Vaccinated Cattle Using Sampling Microneedles. *Sci. Rep.* **2021**, *11*, doi:10.1038/s41598-021-86398-6.
20. Taylor, R.M.; Miller, P.R.; Ebrahimi, P.; Polsky, R.; Baca, J.T. Minimally-Invasive, Microneedle-Array Extraction of Interstitial Fluid for Comprehensive Biomedical Applications: Transcriptomics, Proteomics, Metabolomics, Exosome Research, and Biomarker Identification. *Lab. Anim.* **2018**, *52*, 526–530, doi:10.1177/0023677218758801.
21. Gowers, S.A.N.; Freeman, D.M.E.; Rawson, T.M.; Rogers, M.L.; Wilson, R.C.; Holmes, A.H.; Cass, A.E.; O'Hare, D. Development of a Minimally Invasive Microneedle-Based Sensor for Continuous Monitoring of β-Lactam Antibiotic Concentrations in Vivo. *ACS Sens.* **2019**, *4*, 1072–1080, doi:10.1021/acssensors.9b00288.
22. Li, J.; Wei, M.; Gao, B. A Review of Recent Advances in Microneedle-Based Sensing within the Dermal ISF That Could Transform Medical Testing. *ACS Sens.* **2024**, *9*, 1149–1161, doi:10.1021/acssensors.4c00142.
23. Wilkirson, E.C.; Li, D.; Lillehoj, P.B. Lateral Flow-Based Skin Patch for Rapid Detection of Protein Biomarkers in Human Dermal Interstitial Fluid. *ACS Sens.* **2024**, *9*, 5792–5801, doi:10.1021/acssensors.4c00956.
24. Aroche, A.F.; Nissan, H.E.; Daniele, M.A. Hydrogel-Forming Microneedles and Applications in Interstitial Fluid Diagnostic Devices. *Adv. Healthc. Mater.* **2025**, *14*, doi:10.1002/adhm.202401782.
25. Laszlo, E.; De Crescenzo, G.; Nieto-Argüello, A.; Banquy, X.; Brambilla, D. Superswelling Microneedle Arrays for Dermal Interstitial Fluid (Prote)Omics. *Adv. Funct. Mater.* **2021**, *31*, doi:10.1002/adfm.202106061.
26. Caffarel-Salvador, E.; Brady, A.J.; Eltayib, E.; Meng, T.; Alonso-Vicente, A.; Gonzalez-Vazquez, P.; Torrisi, B.M.; Vicente-Perez, E.M.; Mooney, K.; Jones, D.S.; et al. Hydrogel-Forming Microneedle Arrays Allow Detection of Drugs and Glucose In Vivo: Potential for Use in Diagnosis and Therapeutic Drug Monitoring. *PLOS ONE* **2015**, *10*, e0145644, doi:10.1371/journal.pone.0145644.
27. Al Sulaiman, D.; Chang, J.Y.H.; Bennett, N.R.; Topouzi, H.; Higgins, C.A.; Irvine, D.J.; Ladame, S. Hydrogel-Coated Microneedle Arrays for Minimally Invasive Sampling and Sensing of Specific Circulating Nucleic Acids from Skin Interstitial Fluid. *ACS Nano* **2019**, *13*, 9620–9628, doi:10.1021/acsnano.9b04783.
28. Ranamukhaarachchi, S.A.; Lehnert, S.; Ranamukhaarachchi, S.L.; Sprenger, L.; Schneider, T.; Mansoor, I.; Rai, K.; Häfeli, U.O.; Stoeber, B. A Micromechanical Comparison of Human and Porcine Skin before and after Preservation by Freezing for Medical Device Development. *Sci. Rep.* **2016**, *6*, doi:10.1038/srep32074.
29. Suurs, P.; Van Den Brand, H.; Ten Have, R.; Daamen, W.F.; Barbut, S. Evaluation of Cattle Skin Collagen for Producing Co-Extrusion Sausage Casing. *Food Hydrocoll.* **2023**, *140*, 108595, doi:10.1016/j.foodhyd.2023.108595.
30. Jung, E.C.; Maibach, H.I. Animal Models for Percutaneous Absorption. *J. Appl. Toxicol.* **2015**, *35*, 1–10, doi:10.1002/jat.3004.
31. Todo, H. Transdermal Permeation of Drugs in Various Animal Species. *Pharmaceutics* **2017**, *9*, 33, doi:10.3390/pharmaceutics9030033.
32. Renaudeau, D.; Leclercq-Smekens, M.; Herin, M. Differences in Skin Characteristics in European (Large White) and Caribbean (Creole) Growing Pigs with Reference to Thermoregulation. *Anim. Res.* **2006**, *55*, 209–217, doi:10.1051/animres:2006012.
33. Simon, J.; Mailley, P.; Pin, D.; Mailley, S.; Alava, T.; Ferlay, A.; Blanc, F. Determination of an Implantation Area for Interstitial Fluid Extraction in Cows and Feasibility of Adapted Microneedles. *Biosyst. Eng.* **2022**, *222*, 62–70, doi:10.1016/j.biosystemseng.2022.07.007.
34. Hamid, M.A.; Husain, S.M.I.; Khan, M.K.I.; Islam, M.N.; Biswas, M.A.A. Skin Thickness in Relation to Milk Production of Crossbred Cows. *Pak. J. Biol. Sci.* **2000**, *3*, 1525–1529, doi:10.3923/pjbs.2000.1525.1529.
35. Dowling, D. The Thickness of Cattle Skin. *Aust. J. Agric. Res.* **1955**, *6*, 776, doi:10.1071/ar9550776.

 doi:10.20944/preprints202507.2400.v1

36. Darmau, B.; Hoang, A.; Gross, A.J.; Texier, I. Water-Based Synthesis of Dextran-Methacrylate and Its Use to Design Hydrogels for Biomedical Applications. *Eur. Polym. J.* **2024**, *221*, 113515, doi:10.1016/j.eurpolymj.2024.113515.
37. Kozlowska, J.; Pauter, K.; Sionkowska, A. Carrageenan-Based Hydrogels: Effect of Sorbitol and Glycerin on the Stability, Swelling and Mechanical Properties. *Polym. Test.* **2018**, *67*, 7–11, doi:10.1016/j.polymertesting.2018.02.016.
38. Palencia, M.S.; Mora, M.A.; Palencia, S.L. Biodegradable Polymer Hydrogels Based in Sorbitol and Citric Acid for Controlled Release of Bioactive Substances from Plants (Polyphenols). *Curr. Chem. Biol.* **2017**, *11*, 36–43, doi:10.2174/2212796810666161028114432.
39. Sabri, A.H.B.; Anjani, Q.K.; Donnelly, R.F. Synthesis and Characterization of Sorbitol Laced Hydrogel-Forming Microneedles for Therapeutic Drug Monitoring. *Int. J. Pharm.* **2021**, *607*, 121049, doi:10.1016/j.ijpharm.2021.121049.
40. Li, H.; Wu, G.; Weng, Z.; Sun, H.; Nistala, R.; Zhang, Y. Microneedle-Based Potentiometric Sensing System for Continuous Monitoring of Multiple Electrolytes in Skin Interstitial Fluids. *ACS Sens.* **2021**, *6*, 2181–2190, doi:10.1021/acssensors.0c02330.
41. Darmau, B.; Sacchi, M.; Texier, I.; Gross, A.J. Self-Extracting Dextran-Based Hydrogel Microneedle Arrays with an Interpenetrating Bioelectroenzymatic Sensor for Transdermal Monitoring with Matrix Protection. *Adv. Healthc. Mater.* **2025**, *14*, doi:10.1002/adhm.202403209.
42. Davis, S.P.; Landis, B.J.; Adams, Z.H.; Allen, M.G.; Prausnitz, M.R. Insertion of Microneedles into Skin: Measurement and Prediction of Insertion Force and Needle Fracture Force. *J. Biomech.* **2003**, *37*, 1155–1163, doi:10.1016/j.jbiomech.2003.12.010.
43. Larrañeta, E.; Moore, J.; Vicente-Pérez, E.M.; González-Vázquez, P.; Lutton, R.; Woolfson, A.D.; Donnelly, R.F. A Proposed Model Membrane and Test Method for Microneedle Insertion Studies. *Int. J. Pharm.* **2014**, *472*, 65–73, doi:10.1016/j.ijpharm.2014.05.042.
44. Romgens, A.M.; Bader, D.L.; Bouwstra, J.A.; Baajiens, F.P.T.; C.W.J.Oomens Monitoring the Penetration Process of Single Microneedles with Varying Tip Diameters. *J. Mech. Behav. Bomedical Devices* **2014**, 397–405, doi:.org/10.
45. Chua, B.; Desai, S.P.; Tierney, M.J.; Tamada, J.A.; Jina, A.N. Effect of Microneedles Shape on Skin Penetration and Minimally Invasive Continuous Glucose Monitoring in Vivo. *Sens. Actuators Phys.* **2013**, *203*, 373–381, doi:10.1016/j.sna.2013.09.026.
46. Wei, J.Cj.; Cartmill, I.D.; Kendall, M.Af.; Crichton, M.L. In Vivo, in Situ and Ex Vivo Comparison of Porcine Skin for Microprojection Array Penetration Depth, Delivery Efficiency and Elastic Modulus Assessment. *J. Mech. Behav. Biomed. Mater.* **2022**, *130*, 105187, doi:10.1016/j.jmbbm.2022.105187.
47. Knox, F.S.; Wachtel, T.L.; McCahan, G.R.; Knapp, S.C. Thermal Properties Calculated from Measured Water Content as a Function of Depth in Porcine Skin. *Burns* **1986**, *12*, 556–562, doi:10.1016/0305-4179(86)90005-7.